Frequency-domain wide-field laser Doppler *in vivo* imaging

M. Atlan and M. Gross

Laboratoire Kastler-Brossel, UMR 8552 (ENS, CNRS, UMPC), Ecole Normale Supérieure, 10 Rue Lhomond F-75231, Paris Cedex 05, France

B. C. Forget

Laboratoire d'Optique, École Supérieure de Physique et de Chimie Industrielles de la Ville de Paris, CNRS UPR A0005, Université Pierre et Marie Curie, 10 Rue Vauquelin F-75231, Paris Cedex 05, France

T. Vitalis and A. Rancillac

Laboratoire de Neurobiologie et Diversité Cellulaire, École Supérieure de Physique et de Chimie Industrielles de la Ville de Paris, CNRS UMR 7637, 10 Rue Vauquelin F-75231, Paris Cedex 05, France

A. K. Dunn

Biomedical Engineering Department, University of Texas at Austin, ENS 1 University Station, CO 800, Austin, Texas 78712-0238

We present a new instrument, based on a low-frame-rate (8 Hz) CCD camera used in a heterodyne optical-mixing configuration, that can create wide-field laser Doppler maps. As an illustration, we show results obtained in a mouse brain, *in vivo*, showing the Doppler signature of blood flow. The instrument is based on a frequency-shifting digital holography scheme. © 2006 Optical Society of America

OCIS codes: 170.3340, 170.6480, 090.2880.

Imaging blood flow is an essential tool to assess many physiological processes and diseases. Several instruments to produce blood flow maps have been proposed. These instruments can be grouped in two categories: those that are based on time-domain measurements (laser Doppler techniques) and those based on spatial-domain-measurements (speckle contrast analysis techniques).[1,2] The first laser Doppler experiment is attributed to Yeh and Cummins,[3] who measured the frequency shift of light scattered by moving particles with a spectrometer.

Recently, Serov and co-workers proposed[4] and designed[5,6] a full-field laser Doppler imaging technique based on the acquisition of a sequence of images by a fast complimentary metal oxide semiconductor detector. This method requires, on the one hand, a frame rate high enough to set the cutoff frequency of the restorable spectrum higher than the ones induced by typical blood flow, e.g., ~20 kHz in Ref. 6, and, on the other hand, a sequence of images large enough to reach a 50 Hz spectral resolution.[5]

Laser speckle contrast analysis[7] has been proposed as an alternative to scanning laser Doppler imaging as a full-field imaging technique. In this technique, the first-order spatial statistics of the speckle pattern are used to form blood flow images. It has been successfully used in applications including noninvasive skin capillary blood flow imaging[8] and functional brain imaging.[1]

Laser Doppler and speckle contrast analysis turn out to be based on the same underlying phenomenon.[2,9–11] A new experimental approach is proposed here, consisting of a frequency-domain measurement onto a parallel detector. This measurement is based on an optical-mixing scheme.

The setup consists of a heterodyne measurement of scattered (object) optical field E_O. The object is illuminated over an ~1 cm × 1 cm area (the region to be imaged). The backscattered laser wave is mixed with a frequency-shifted local oscillator (LO) E_{LO} field. Laser light is provided by a 658 nm (angular frequency ω_L), 80 mW CW Mitsubishi ML120G21 single-mode diode. Two Bragg cells (acousto-optic modulators), are used as beam frequency shifters (see Fig. 1). The LO angular frequency ω_{LO} is shifted by the difference $\Delta\omega_{AOM}$ in driving frequencies of the set of Bragg cells: $\omega_{LO} = \omega_L + \Delta\omega_{AOM}$. A 1.3 Mpixel PCO PixelFly camera (frame rate ω_S, square pixels, pixel size 6.7 μm) is used to record a sequence of m images (namely, I_k, where $k = 1, \ldots, m$) of the interference pattern resulting from optical mixing between the LO and object fields. The detection plane is set 50 cm from the object plane. A circular pupil set in front of the object limits the field of view. Since the spatial field of interest in the object is ≈1 cm², it matches the natural heterodyne parallel detection image field, avoiding the need for any lens in the object path.

The optical configuration is a typical holographic setup, called a lensless Fourier (off-axis) holography setup,[12,13] in which the point source of the spherical reference wave (LO focal point) is located in the plane of the object. The lensless Fourier setup is used to avoid the need for a general Fresnel reconstruction algorithm[14] to assess the spatial distribution of the
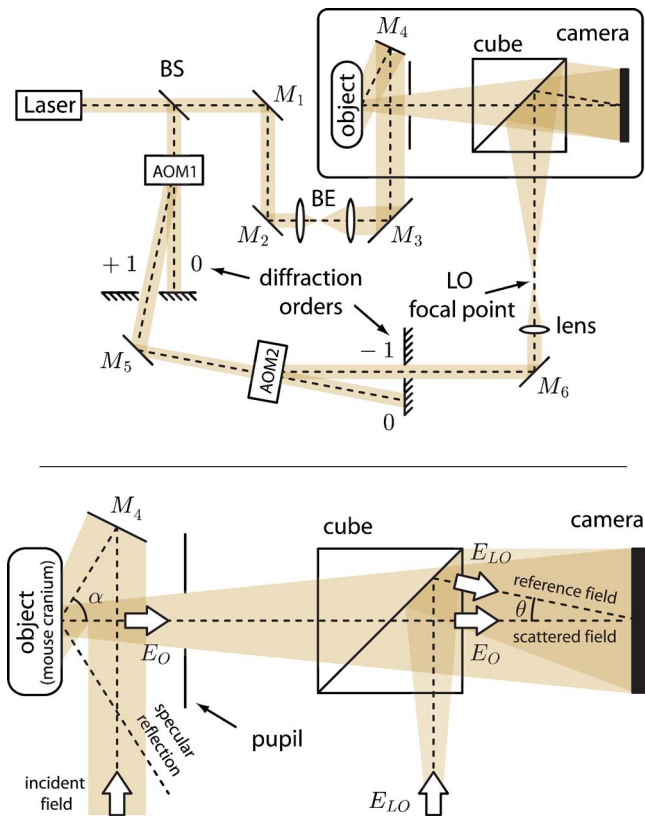
Fig. 1. (Color online) Optical configuration (top, general view; the inset is enlarged in the bottom part). AOMs,1,2, Bragg cells; BS, beam splitter; BE, beam expander. M_1–M_6, mirrors; E_O, object (scattered) field; E_{LO}, reference (LO) field.

scattered field in the object plane. In this case, the reconstruction algorithm consists of only one spatial fast Fourier transform (FFT).[13]

The digital hologram is recorded according to the frequency-shifting method introduced in the heterodyne holography technique, used in several imaging and detection schemes,[15–18] which turns out to be sensitive enough to discriminate Doppler-shifted photons, according to their frequency, from background light.[16,18] The frequency-shifting method was chosen as an accurate[15] phase-shifting[19] detection method.

To create a map of the $\Delta\omega$ angular frequency component [corresponding to the $\Delta f = \Delta\omega/(2\pi)$ frequency, in Hz] of the scattered field in the image plane, the LO frequency is set to $\omega_{LO} = \omega_L + \Delta\omega + \omega_S/n$, where the integer n satisfies $n \geq 2$.

The power $S(\omega = \omega_L + \Delta\omega)$ of the $\Delta\omega$ frequency component of the measured object field is computed in parallel on the pixels of the image, according to the n-phase demodulation method.[16,17] This method consists of calculating the squared amplitude of the ω_S/n AC component of intensity fluctuations I_k by a time-domain FFT: $S(\omega) = A|\sum_{k=1}^{n} I_k \exp(1 - 2j(k-1)\pi/n)|^2$, where A is a constant and $j^2 = -1$.

In the reported experiment, the cranium of a mouse is illuminated with an incidence angle $\alpha \approx 60°$. The angle between the object and LO arms is set to $\theta \approx 1°$. This experiment was designed to deter-

mine whether the instrument would allow detection of the cerebrocortical blood flow.

Animal procedures were conducted in strict compliance with approved institutional protocols and in accordance with the provisions for animal care and use described in the European Communities Council directive of November 24, 1986 (86-16-09/EEC). Five C57/B16 mice (Charles River) aged P25–P30 were anesthetized with a mixture of xylazine–ketamine (1 mg/kg IP, 10 mg/kg IP). Animals were positioned on a stereotaxic frame (World Precision Instruments) to ensure stability of the preparation. Cranial skin and subcutaneous tissue were excised linearly over the sagittal suture and cortical bones were preserved.

To assess bioflow,[20] the root mean square (RMS) frequency shift $\langle\Delta\omega^2\rangle^{1/2}$ was calculated with respect to the $S(\omega)$ distribution measured at 80 linearly spaced frequency points in the 0–2528 Hz range (spacing interval 32 Hz). The camera frame rate was set to 8 Hz. A sequence of $m = 32$ images sampled during 32/8 = 4 s was taken to build each $S(\omega = \omega_L + \Delta\omega)$ map at one given $\Delta\omega$ frequency point, setting $\Delta\omega_{AOM} = \Delta\omega + \omega_S/n$, where $n = 4$. To increase the signal-to-noise ratio, $S(\omega)$ was averaged by means of an accumulation of sliding n-phase demodulation along the m image sequence. The whole measurement took 5:20 (=32 images × 80 frequency shifts
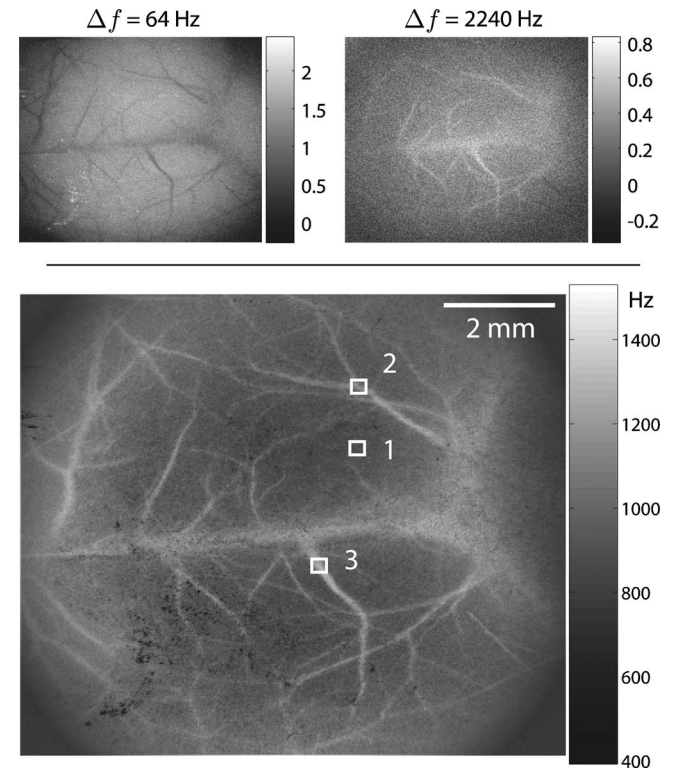

Fig. 2. Power maps of the $\Delta f = 64$ Hz and $\Delta f = 2240$ Hz frequency components of the scattered field (top, log scale) and the perfusion map, i.e., the RMS frequency shift, in hertz (bottom). A mouse cranium (from which the skin and subcutaneous tissue were excised) is observed in retrodiffusion configuration (Fig. 1), *in vivo*. The image shows a dorsal view of the mouse cranium (anterior on the left, posterior on the right). The superficial dorsal venous system and some of the superficial cerebral arteries are visible (squares labeled 1–3).
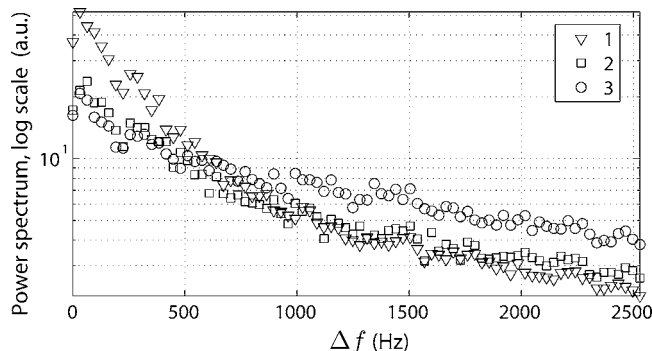
Fig. 3. Spectra calculated in the three 5×5 pixel ROI outlined in Fig. 2 (log scale).
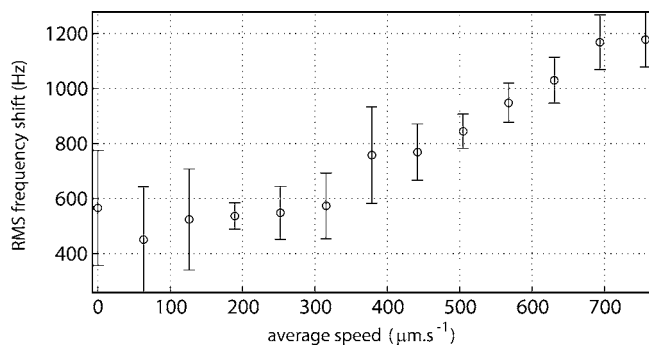

Fig. 4. *In vitro* measurement of the light scattered by a 5×10^{-3} volume fraction suspension of $1\,\mu$m latex beads flowing through a transparent tube of $580\,\mu$m diameter. The average RMS frequency shift versus average speed of flow is shown.

$\times 1/8$ exposure time). Two $S(\omega)$ spatial maps at a low ($\Delta f = 64$ Hz) and a higher ($\Delta f = 2240$ Hz) frequency shift and a spatial map of the RMS frequency shift (in hertz) are represented in Fig. 2. Three spectra, averaged over 5×5 pixel regions of interest (ROI, outlined in Fig. 2), are displayed in Fig. 3. The larger blood vessels (e.g., ROI 3) induce a broader spectrum than the smaller ones (ROI 2). In the parenchyma (ROI 1), the spectra are narrower, suggesting reduced blood perfusion, hence the contrast reversal between the two spectral maps in Fig. 2. An additional *in vitro* calibration experiment was done to assess the order of magnitude of the measured RMS frequency shift for various flow rates. The result is shown in Fig. 4; it demonstrates an approximately linear relationship between the average speed (from 0 to 750 μm s^{-1}) and the measured frequency shift.

In conclusion, this scheme based on heterodyne optical mixing onto a parallel detector is particulary suited to wide-field laser Doppler imaging. An arbitrary frequency component of the object field can be acquired at once. The available range of frequency shifts at which measurements can be made is far more extended than in any of the concurrent techniques, since the measurement is performed directly in the frequency domain. The actual limit, lies in the system used to shift the LO frequency. As an indica-

tion, the RF-driven acousto-optic modulator combination can shift this frequency up to 10 MHz.

The measurement is sensitive: because of the off-axis holographic setup, the low-frequency noise components (homodyne intensity terms, resulting from laser instabilities and scattered light self-interference) within the camera bandwidth are efficiently filtered out.[16,17]

The Doppler map is not restored over the total number of pixels of the camera. Only up to 1/4 of the pixels of the frame can be used to describe the image, as a result of the off-axis holographic scheme. Nevertheless, both temporal and spatial resolution are potentially high. This combination is enabled by a measurement performed at one frequency point at a time.

A faster camera could be used to improve temporal resolution and still keep a spectral resolution that is acceptable for this measurement, since the spectral resolution is defined by the heterodyne bandwidth (inverse of the acquisition time). A detection array with a large number of pixels should be used to perform efficient wide-field and high-spatial-resolution detection. Due to the data transfer rate limit encountered, the balance between the number of pixels and the frame rate of the detector should be guided by the application needs in terms of temporal, spectral, and spatial resolution.

M. Atlan's e-mail address is atlan@lkb.ens.fr.

References

1. A. Dunn, H. Bolay, M. A. Moskowitz, and D. A. Boas, J. Cereb. Blood Flow Metab. **21**, 195 (2001).
2. T. Yoshimura, J. Opt. Soc. Am. A **3**, 1032 (1986).
3. Y. Yeh and H. Z. Cummins, Appl. Phys. Lett. **4**, 176 (1964).
4. A. Serov, W. Steenbergen, and F. de Mul, Opt. Lett. **27**, 300 (2002).
5. A. Serov, B. Steinacher, and T. Lasser, Opt. Express **13**, 3681 (2005).
6. A. Serov and T. Lasser, Opt. Express **13**, 6416 (2005).
7. A. F. Fercher and J. D. Briers, Opt. Commun. **37**, 326 (1981).
8. J. D. Briers, G. Richards, and X. W. He, J. Biomed. Opt. **4**, 164 (1999).
9. J. D. Briers, Physiol. Meas **22**, R35 (2001).
10. R. Bonner and R. Nossal, Appl. Opt. **20**, 2097 (1981).
11. J. A. Briers, J. Opt. Soc. Am. A **13**, 345 (1996).
12. U. Schnars and W. P. O. Juptner, Meas. Sci. Technol. **13**, R85 (2002).
13. C. Wagner, S. Seebacher, W. Olsten, and W. Juptner, Appl. Opt. **38**, 4812 (1999).
14. U. Schnars, J. Opt. Soc. Am. A **11**, 2011 (1994).
15. F. LeClerc, L. Collot, and M. Gross, Opt. Lett. **25**, 716 (2000).
16. M. Gross, P. Goy, B. C. Forget, M. Atlan, F. Ramaz, A. C. Boccara, and A. K. Dunn, Opt. Lett. **30**, 1357 (2005).
17. M. Atlan, B. C. Forget, F. Ramaz, A. C. Boccara, and M. Gross, Opt. Lett. **30**, 1360 (2005).
18. M. Gross, P. Goy, and M. Al-Koussa, Opt. Lett. **28**, 2482 (2003).
19. I. Yamaguchi and T. Zhang, Opt. Lett. **18**, 31 (1997).
20. P. Starukhin, S. Ulyanov, E. Galanzha, and V. Tuchin, Appl. Opt. **39**, 2823 (2000).